

CONVERGENCE DYNAMICS OF AGENT-TO-AGENT INTERACTIONS WITH MISALIGNED OBJECTIVES

Romain Cosentino

Salesforce AI Research
rcosentino@salesforce.com

Sarath Shekkizhar

Salesforce AI Research
sshekkizhar@salesforce.com

Adam Earle

Salesforce AI Research
aearle@salesforce.com

ABSTRACT

We develop a theoretical framework for agent-to-agent interactions in multi-agent scenarios. We consider the setup in which two language model based agents perform iterative gradient updates toward their respective objectives in-context, using the output of the other agent as input. We characterize the generation dynamics associated with the interaction when the agents have misaligned objectives, and show that this results in a biased equilibrium where neither agent reaches its target - with the residual errors predictable from the objective gap and the geometry induced by the prompt of each agent. We establish the conditions for asymmetric convergence and provide an algorithm that provably achieves an adversarial result, producing one-sided success. Experiments with trained transformer models as well as GPT5 for the task of in-context linear regression validate the theory. Our framework presents a setup to study, predict, and defend multi-agent systems; explicitly linking prompt design and interaction setup to stability, bias, and robustness.

1 INTRODUCTION

Large language models (LLMs) increasingly act as *agents* that exchange messages, propose edits, and iteratively refine solutions in multi-step workflows (Mohammadi et al., 2025; Niu et al., 2025; Zhang et al., 2025). While this trend has spurred a surge of multi-agent designs, from debate and role-structured discussions to autonomous tool-using collectives (Wu et al., 2024; Du et al., 2023; Liang et al., 2024; Chen et al., 2023), their behavior remains difficult to predict, especially when agent goals are only partially aligned (Erisken et al., 2025; Altmann et al., 2024; Cemri et al., 2025). Recent empirical findings further caution that, under common prompting and coordination schemes, multi-agent setups may not consistently outperform strong single-agent baselines and can be brittle and unreliable participants (Wang et al., 2024; Huang et al., 2025a; Wynn et al., 2025; Lee & Tiwari, 2024). These observations motivate a principled, mechanistic account of how interacting LLM agents update their internal states *because of* each other.

Our analysis builds on an emerging theoretical view of LLM inference as *in-context optimization*. A growing body of work shows that sufficiently trained transformers can implement algorithmic updates, including gradient descent for linear regression tasks, using only the information provided in the prompt (Akyurek et al., 2023; Garg et al., 2022; von Oswald et al., 2023; Ahn et al., 2023; Dai et al., 2022). Most relevant to us, Huang et al. (2025b) prove that a single-layer transformer with linear self-attention (LSA) can carry out *multiple* gradient-descent-like steps in context when trained to predict the next iterate on quadratic objectives. We adopt this insight as a modeling primitive: specifically, we assume that once appropriately trained, each agent performs a stable, approximately linear *gradient* update towards its own objective, from the incoming context (representing the previous iterate).

Building on this “transformers-as-optimizers” perspective, we theoretically investigate *agent-to-agent* interactions as an *alternating optimization* process between two LSA agents with potentially

misaligned objectives. Concretely, at each turn an agent consumes the other’s latest iterate and applies a gradient update towards its own objective. This yields a coupled dynamical system whose fixed points need not coincide with either agent’s ground truth objective. Our analysis shows that the limiting biases are jointly governed by (i) **objective misalignment** (the discrepancy between objectives) and (ii) **prompt geometry anisotropy** (spectral structure of agent-specific covariances that shape update directions). Notably, anisotropy induces directional filtering: the residual of each agent is amplified in directions dominated by the *other* agent’s geometry.

We also analyze the conditions under which the agent-to-agent dynamics admit *asymmetric convergence*: where one agent can attain its objective exactly while the other is left with a persistent bias. These conditions translate into constructive mechanisms for *adversarial prompt design* that cancel an opponent’s corrective directions while preserving the attacker’s progress. This connects predictive modeling to concrete security concerns for multi-agent LLM systems (He et al., 2025; Struppek et al., 2024; Xi et al., 2023; Wang et al., 2023).

We validate the theory with experiments using trained LSA agents in the sense of Huang et al. (2025b). We also provide experimental validations with GPT5 for our adversarial prompt design approach. Importantly, when objectives align, the shared iterate converges cooperatively to the common objective. Under misalignment, both agents plateau at analytically predicted, generally *unequal* residuals that grow with the inter-objective angle. Under adversarial designs derived from our kernel criteria, we observe reliable asymmetric outcomes: the attacker converges to its objective while the victim remains biased.

Our contributions are summarized as follows: (i) We formalize agent-to-agent interactions as alternating, in-context gradient updates between two transformer agents (Section 2). (ii) We obtain closed-form expressions for each agent’s limiting error that depends on objective misalignment and prompt anisotropy. We also include spectral analysis of the error and derive error bounds with respect to the angle between the objectives (Section 3). (iii) We establish kernel conditions for *asymmetric convergence* and give a constructive adversarial geometry that enforces it leading to a white-box attack procedure (Section 4). (iv) We corroborate these theoretical results with trained LSA agents as well as GPT5 experiments, highlighting when and how multi-agent interactions can be helpful, when they result in agent compromises, and when they can be steered to harmful outcomes. While the experiments are provided throughout the paper, experimental details are given in Section 5.

Overall, our results bridge mechanistic accounts of in-context learning with the design and safety of multi-agent LLM systems. We provide simple spectral diagnostics and actionable constructions that we hope will help shape a better understanding of robust multi-agent LLM deployments.

2 AGENT-TO-AGENT FORMALISM

In this section we develop a formal model of *agent-to-agent* interactions grounded in the emerging view of LLM inference as *in-context optimization*. Rather than analyzing prompting procedures directly, we consider that each agent realizes a *gradient* update on its own objective from the received context. This assumption is supported by theory and experiments showing that trained transformers can implement algorithmic updates, including multi-step gradient descent for quadratic objectives, purely in context; in particular, Huang et al. (2025b) establish such behavior for single-layer LSA.

We first recall the single-agent setting in which an LSA model, given a dataset packaged as tokens, emits successive iterates that track gradient descent on a least square regression problem. We then lift this formalism to propose a theoretical backbone to agent-to-agent interactions. In such case, which each agent has its own set of weights, and a specific prompt dependent on its linear regression objective. The agents interact by alternating turns; each consuming the other’s latest iterate and applying its own in-context update toward its objective. The result is a coupled, turn-by-turn dynamical system amenable to fixed-point and spectral analysis. This agent-to-agent framing allows us to quantify how *objective misalignment* and *prompt geometry* jointly determine convergence, plateaus, and potential asymmetries.

2.1 IN CONTEXT OPTIMIZATION

Chain-of-Thought (CoT) prompting (Wei et al., 2022) enables large language models to break down complex reasoning into intermediate steps, significantly improving performance on mathematical and logical tasks. Recent theoretical work has revealed the optimization foundations underlying this process. Huang et al. (2025b) provide a theoretical analysis of how transformers can learn to implement iterative optimization through CoT prompting. They consider a linear regression task within the in-context learning (ICL) framework and demonstrate that a suitably trained transformer can perform multiple steps of gradient descent on the mean squared error objective.

The data consist of n example input-output pairs from a linear model,

$$w^* \sim \mathcal{N}(0, I_d), \quad x_i \sim \mathcal{N}(0, I_d), \quad y_i = x_i^\top w^* \quad \text{for } i = 1, \dots, n.$$

The learner is given these examples in context and must estimate the underlying weight vector w^* (without further gradient updates to its own weights). The key insight is that a transformer can use CoT to iteratively refine an internal estimate of w^* over k autoregressive steps.

The LLM is modeled as a single-layer LSA transformer with residual connections. The input to the LSA is as follows:

$$Z = \begin{bmatrix} x_1 & \cdots & x_n & 0 \\ y_1 & \cdots & y_n & 0 \\ 0 & \cdots & 0 & w_0 \\ 0 & \cdots & 0 & 1 \end{bmatrix} := \begin{bmatrix} X & 0 \\ y & 0 \\ 0_{d \times n} & w_0 \\ 0_{1 \times n} & 1 \end{bmatrix} \in \mathbb{R}^{d_e \times (n+1)},$$

where $X = [x_1, \dots, x_n]^\top \in \mathbb{R}^{n \times d}$ is the data matrix, $w_0 = 0_d$ is the initialization of the objective weight, and $d_e = 2d + 2$. Note that the token matrix Z encodes input data (x_i, y_i) and also includes dimensions to autoregressively represent the current weight estimate.

The LSA mapping is defined as:

$$f_{\text{LSA}}(Z; V, A) = Z + VZ \cdot \frac{Z^\top AZ}{n},$$

where $V, A \in \mathbb{R}^{d_e \times d_e}$ are learned weight matrices. The model’s prediction is the embedding of the final token

$$w = f_{\text{LSA}}(Z)[:, -1].$$

With appropriate training, the LSA transformer learns to output a sequence of weight estimates $\{w_0, w_1, \dots, w_k\}$ where each CoT step approximates a gradient descent update,

$$w_{t+1} \approx w_t - \eta \frac{1}{n} X^\top (X w_t - y), \quad (1)$$

with $\eta > 0$ the learning rate. In other words, at each CoT step, the LSA transformer performs a gradient descent step on the least square loss $\frac{1}{2} \|Xw - y\|^2$ with respect to its previous weight estimate.

2.2 AGENT-TO-AGENT FORMULATION

We now extend this framework to agent-to-agent interactions under an alternating turn-taking protocol. In this setting, two agents engage in a dialogue where, at each turn, an agent receives as input the prompt and accumulated conversation history, and subsequently generates an output response.

Consider two agents, W and U , that alternate turns: each agent receives the other’s output and performs one step toward its own objective. Following the aforementioned linear regression formalism, we consider the following data structure at turn t ,

$$Z_W = \begin{bmatrix} X_W & 0 \\ y_W & 0 \\ 0_{d \times n} & u_0, w_1, u_1, \dots, u_{t-1} \\ 0_{1 \times n} & 1 \end{bmatrix}, \quad Z_U = \begin{bmatrix} X_U & 0 \\ y_U & 0 \\ 0_{d \times n} & u_0, w_1, u_1, \dots, u_{t-1}, w_t \\ 0_{1 \times n} & 1 \end{bmatrix},$$

In this construction, agent W utilizes (X_W, y_W) together with the conversation history $[u_0, w_1, u_1, \dots, w_{t-1}, u_{t-1}]$ to produce the update w_t . Now, agent U employs (X_U, y_U) along

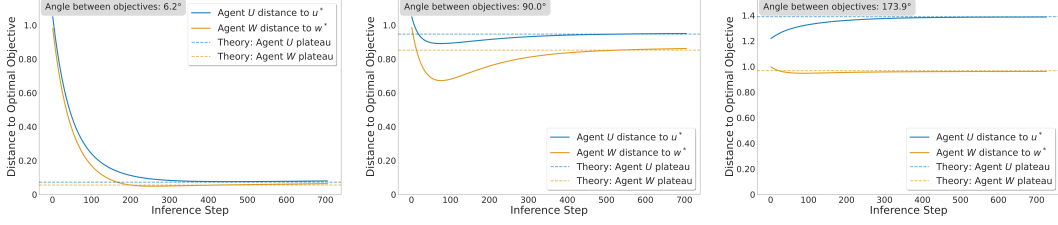


Figure 1: **Plateau error vs objective alignment:** (left) With aligned objectives, both agents converge cooperatively to the shared objective. Note that because of the $\sim 6^\circ$ angle between objective, the agents do not converge to 0-error. (middle) With orthogonal objectives ($\sim 90^\circ$), convergence occurs toward a solution that does not advantage either agent. (right) With opposite ($\sim 174^\circ$) objectives, the dynamic is similar to the orthogonal objective case. Note that (i) whether agent U or agent W converges to a better error is induced by the prompt geometry, and (ii) in all cases here, neither agent converges to a 0-error solution. These two key points are central to the characterization we provide in Section 3.

with the extended history $[u_0, w_1, u_1, \dots, w_{t-1}, u_{t-1}, w_t]$ to generate u_t . Note that we default the initialization to $u_0 = 0_d$ and consider that agent W speaks first.

Note that, each agent may have different objectives. In our theory that takes the form of having misaligned regression objectives $w^* \neq u^*$. Building on Huang et al. (2025b), there exists a parametrization of the LSA under which each mapping applied to the input data approximates a gradient descent update. Such a parametrization arises from training the LSA toward the gradient-descent update. All LSA experiments in this paper are inference-only and use LSA agents that were pretrained (in a single-agent setting) to generalize the gradient-prediction task described in Section 2.1.

Consequently, each agent also admits the gradient-descent update defined in Eq. 1. The resulting alternating dynamics between the two agents that will be central to this paper are given by

$$w_{t+1} = u_t - \eta S_W (u_t - w^*) \quad (2)$$

$$u_{t+1} = w_{t+1} - \eta S_U (w_{t+1} - u^*), \quad (3)$$

where $S_W = \frac{1}{n} X_W^\top X_W$ and $S_U = \frac{1}{n} X_U^\top X_U$ the covariance matrices of the data. When the agents pursue aligned objectives, i.e., $w^* = u^*$, these alternating updates collapse to the single agent formalism as defined in Huang et al. (2025b). *In contrast, when objectives are misaligned ($w^* \neq u^*$), the agent-to-agent dynamics may give rise to different behaviors, including mutual convergence, asymmetric convergence (where one agent achieves its objective while persistently biasing the other), or adversarial interactions in which one agent systematically manipulates the trajectory of the conversation.* The remainder of the paper is devoted to analyzing these interactions at inference given trained models.

3 AGENT-TO-AGENT DYNAMICS

In this section, we analyze the agent-to-agent update dynamics and derive *explicit* expressions for the errors between each agent’s iterate and its respective objective. These results characterize the unequal convergence plateaus obtained when two agents interact (see Figure 1). We will assume a fixed point convergence for these equations which is a condition on the gradient descent learning rate (see Appendix 8.1 for more details).

The following proposition characterize asymptotic errors of each agent from their respective objectives as a result of turn-base agent-to-agent interaction at inference with a trained LSA model.

Proposition 1. *Let $S := S_W + S_U$ be invertible and let $\Delta = u^* - w^*$, then as $\eta \rightarrow 0$,*

$$\|u_\infty - u^*\|_2^2 = \Delta^\top (S_W S^{-2} S_W) \Delta + O(\eta), \quad \|w_\infty - w^*\|_2^2 = \Delta^\top (S_U S^{-2} S_U) \Delta + O(\eta). \quad (4)$$

(Proof in Appendix 8.2)

Assuming S is invertible means that there are no blind directions where the misalignment $\Delta = u^* - w^*$ can hide from both agents. In practice, one ensures invertibility by using sufficiently diverse, non-collinear in-context examples across the two prompts.

This proposition shows that, after sufficiently many turns, each agent’s residual error is governed by two key factors: (i) the discrepancy between the agents’ objectives, and (ii) the structure of their respective prompts. In the linear regression setting, that is, the covariance structure of the data. Note that the squared asymptotic errors capture the smoothness of the objective difference, i.e., Δ , along the spectrum of S_W (resp. S_U) normalized by S . Therefore, the anisotropy of (S_W, S_U) can potentially make these plateaus unequal, leading to agent-to-agent dependent convergences.

In Figure 1, we observe at inference the empirical error of each agent towards their objective as well as the computed theoretical convergence plateau obtained from Proposition 1. Importantly, the asymptotic error can be computed before any agent-to-agent interaction given knowledge of the prompts and the objectives.

The quadratic forms in Proposition 1 highlight that the limiting plateaus are not determined solely by the objective misalignment Δ , but also by the anisotropy of the agents’ prompt geometries (S_W, S_U) . In the isotropic case, where S_W and S_U are multiples of the identity, the weights $S_W S^{-2} S_W$ and $S_U S^{-2} S_U$ collapse to scalars, and both agents experience identical plateau errors proportional to $\|\Delta\|_2^2$. By contrast, when the spectra of S_W and S_U differ across directions, the error decomposition depends on how Δ aligns with the eigenspaces of these respective prompts. The following corollary highlights such behavior.

Corollary 1. Assume S_W and S_U commute so they are simultaneously diagonalizable with eigenvalues Λ_W, Λ_U , and let $\tilde{\Delta}$ be the projection of Δ in their eigenbasis. Then, as $\eta \rightarrow 0$,

$$\|u_\infty - u^*\|_2^2 = \sum_{i=1}^d \left(\frac{\lambda_{w,i}}{\lambda_{w,i} + \lambda_{u,i}} \right)^2 \tilde{\Delta}_i^2 + O(\eta) \quad \|w_\infty - w^*\|_2^2 = \sum_{i=1}^d \left(\frac{\lambda_{u,i}}{\lambda_{w,i} + \lambda_{u,i}} \right)^2 \tilde{\Delta}_i^2 + O(\eta)$$

(Proof in Appendix 8.3)

In the commuting case, the misalignment Δ decomposes into independent spectral directions, and each agent’s plateau is obtained by weighting the per-mode discrepancy $\tilde{\Delta}_i$. Along a mode i where $\lambda_{w,i} \gg \lambda_{u,i}$, the U agent error is *amplified* while that of W agent is *suppressed* and vice versa. Thus anisotropy acts as a directional filter: each agent incurs larger errors precisely in the directions where the other agent’s geometry dominates.

Now that we understand how the prompt and its induced geometry affects each agent’s asymptotic error, we are interested in the impact of objective discrepancy. The following corollary provides a description of the error that each agent will achieve at convergence with respect to the angle between the two objectives.

Corollary 2. Let $S := S_W + S_U$ be invertible, $\theta \in [0, \pi]$ be the angle between w^* and u^* , then as $\eta \rightarrow 0$,

$$\alpha_U r_{\min}(\theta) \leq \frac{\|u_\infty - u^*\|_2}{\sqrt{\|w^*\|_2^2 + \|u^*\|_2^2}} \leq \beta_U r_{\max}(\theta) + O(\eta), \quad (5)$$

$$\alpha_W r_{\min}(\theta) \leq \frac{\|w_\infty - w^*\|_2}{\sqrt{\|w^*\|_2^2 + \|u^*\|_2^2}} \leq \beta_W r_{\max}(\theta) + O(\eta), \quad (6)$$

where

$$r_{\min}(\theta) = \min\{1, \sqrt{1 - \cos \theta}\}, \quad r_{\max}(\theta) = \max\{1, \sqrt{1 - \cos \theta}\},$$

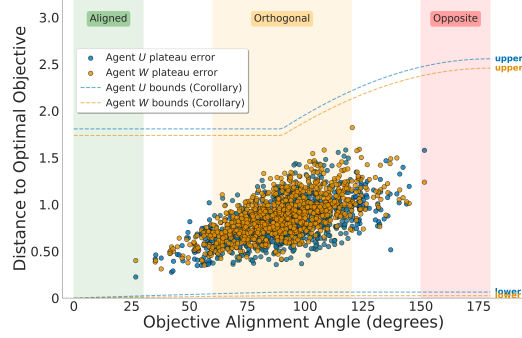


Figure 2: **Plateau error v.s. objective angle** - Plateau error of Agents W (blue) and U (orange) as a function of the objective alignment angle (1000 LSA agent-to-agent interactions). We display the theoretical bounds from Corollary 2 for each agent (lower and upper). As the bounds in Corollary 2 characterize, larger alignment angles correspond to higher plateau errors.

$$\begin{aligned}\alpha_U &= \sqrt{\lambda_{\min}(S_W S^{-2} S_W)}, & \beta_U &= \sqrt{\lambda_{\max}(S_W S^{-2} S_W)}, \\ \alpha_W &= \sqrt{\lambda_{\min}(S_U S^{-2} S_U)}, & \beta_W &= \sqrt{\lambda_{\max}(S_U S^{-2} S_U)}.\end{aligned}$$

(Proof in Appendix 8.4)

From this corollary, the normalized convergence plateaus are *nondecreasing* in $\theta \in [0, \pi]$, bounded between the envelopes $\alpha r_{\min}(\theta)$ and $\beta r_{\max}(\theta)$ (up to an $O(\eta)$ term), with multiplicative constants (α_U, β_U) and (α_W, β_W) for agents U and W , respectively. This phenomena is observed empirically in Figure 2 where we observe each agent’s asymptotic error with respect to the angle between their objective. As formally described in Corollary 2, the plateau error of each agent increases with respect to the angle between their objective.

These results suggest a concrete prompt-design principle for multi-agent systems: *each agent’s prompt should explicitly encode a shared global objective. Without an explicit common objective, CoT generation may instantiate agent-specific local objectives that are partially misaligned, leading to coupled errors and biased outcomes across the interaction.*

In this section, we established explicit expressions for the asymptotic errors of both agents (Proposition 1), showing that convergence plateaus are determined jointly by objective misalignment Δ and the spectral geometry of the prompts (S_W, S_U) . We further derived angle-based bounds (Corollary 2), explaining the growth of normalized plateaus with the inter-objective angle, as observed in Figures 1 and 2. Together, these results enable *a priori* prediction of plateau levels and provide concrete design levers, via the spectra of S_W and S_U , to ensure bounded residuals and mitigate asymmetric vulnerabilities in non-cooperative agent-to-agent interactions.

4 ASYMMETRIC CONVERGENCE AND GEOMETRIC CHARACTERIZATION OF ADVERSARIAL AGENTS

We presently develop a theoretical framework for adversarial agents. Specifically, we first characterize geometric conditions under which *asymmetric convergence* is achievable in an agent-to-agent system. That is, is it possible to tune the interaction, via the choice of prompts, so that one agent converges exactly to its objective, while the other agent does not.

4.1 ASYMMETRIC CONVERGENCE CONDITIONS

The following proposition presents conditions on the fixed-point equations of the system to achieve asymmetric convergence.

Proposition 2. *Asymmetric convergence (i.e., $u_\infty = u^*$ but $w_\infty \neq w^*$) occurs if and only if*

$$\Delta \in \ker((I - \eta S_U) S_W) \quad \text{and} \quad \Delta \notin \ker(\eta S_W - I). \quad (7)$$

(Proof in Appendix 8.5)

The first condition in equation 7 says that the part of the objective gap $\Delta = u^* - w^*$ that W would try to correct is *nullified* by U ’s turn: whatever W injects along Δ through its gradient direction $S_W \Delta$ lands in the nullspace of $(I - \eta S_U)$, so U cancels it and can still steer itself exactly to u^* . The second condition excludes a degenerate “one-step fix” for W (i.e., Δ lying in the eigenspace of S_W with eigenvalue $1/\eta$), which would otherwise let W also eliminate its residual and remove asymmetry. This reasoning can be obtained by looking at the agent-to-agent composed two-turn agent U update

$$u_{t+1} = (I - \eta S_U)w_{t+1} + \eta S_U u^*, \quad w_{t+1} = u_t - \eta S_W(u_t - w^*),$$

Then,

$$\begin{aligned}u_{t+1} &= \eta S_U u^* + (I - \eta S_U)u_t - \underbrace{\eta(I - \eta S_U) S_W (u^* - w^*)}_{= 0 \text{ by Eq. equation 7}} - \eta(I - \eta S_U)S_W(u_t - u^*) \\ &= u_t - \eta[S_U + (I - \eta S_U)S_W](u_t - u^*).\end{aligned}$$

Algorithm 1 White-box Attack - Prompt Design

Require: $S_W \in \mathbb{R}^{d \times d}$, mismatch $\Delta = w^* - u^* \in \mathbb{R}^d$, stability margin $\tau \in (0, 1/2)$ (e.g. 0.1), step size η

Build the line-space and its projector

- 1: Set $v \leftarrow S_W \Delta$.
- 2: Set $P_v \leftarrow \frac{vv^\top}{\|v\|^2}$ (projector onto $\text{span}\{v\}$).

Build the adversarial geometry S_U .

- 3: Pick any $\varepsilon \in (0, 1/\eta)$ (e.g. $\varepsilon \leftarrow \frac{1-\tau}{\eta}$).
- 4: Set

$$S_U \leftarrow \frac{1}{\eta} P_v + \varepsilon (I - P_v).$$

Realize S_U as a data covariance.

- 5: Factor S_U as $S_U = LL^\top$.
 - 6: Form $X_\Gamma \in \mathbb{R}^{d \times n}$ with columns spanning $\text{Im}(L)$, e.g. $X_\Gamma \leftarrow \sqrt{n} L$.
 - 7: **return** X_U, η .
-

Similarly we can decompose agent W next-step error to obtain

$$\begin{aligned} w_{t+1} - w^* &= (I - \eta S_W)(u_t - w^*) \\ &= (I - \eta S_W)(u_t - u^*) + \underbrace{(I - \eta S_W)\Delta}_{\text{misalignment term}}. \end{aligned}$$

If Δ is an eigenvector of S_W with eigenvalue $1/\eta$, then $(I - \eta S_W)\Delta = 0$, so W eliminates its residual along that misalignment direction, therefore undoing the asymmetry.

Now we propose to leverage these conditions to provide a provable asymmetric convergence construction.

Corollary 3. *Let $\Delta \neq 0$ and choose $\eta > 0$ such that $(\frac{1}{\eta}, \Delta) \notin \text{spec}(S_W)$. Define $v := S_W \Delta$ and let P_v denote the orthogonal projector onto $\text{span}\{v\}$. Set*

$$S_U = \frac{1}{\eta} P_v + \varepsilon (I - P_v) \quad \text{for any } \varepsilon \in (0, \frac{1}{\eta}).$$

Then the agent-to-agent dynamics exhibit asymmetric convergence: agent U reaches its objective while agent W does not. (Proof in Appendix 8.6)

The construction sets S_U to place an *eigenvalue spike* exactly on the problematic direction $v := S_W \Delta$ and to be near-isotropic elsewhere. Because $S_U v = \frac{1}{\eta} v$, we get

$$(I - \eta S_U)v = 0 \quad \implies \quad (I - \eta S_U)S_W \Delta = 0,$$

which satisfies the kernel criterion in Proposition 2. The small $\varepsilon(I - P_v)$ term makes S_U full-rank for stability while keeping U 's behavior essentially unchanged on $\text{span}\{v\}$. The side condition $(\frac{1}{\eta}, \Delta) \notin \text{spec}(S_W)$ prevents a symmetric one-step elimination for W .

4.2 WHITE-BOX AGENT-TO-AGENT ATTACK

In the white-box setting, the adversarial agent has complete knowledge of the target agent's geometry matrix S_W and objective w^* . Note that this scenario is realistic as one can either perform prompt extraction techniques (Zou et al., 2023; Yang et al., 2024; Li et al., 2025) or simply by guessing the other agent prompt and objective prior to the agent-to-agent interaction.

Given knowledge of (S_W, w^*, u^*) , the attacker's goal is to construct an optimal attack geometry S_U such that the agent-to-agent conversation converges to the attacker's objective u^* while preventing the victim from reaching w^* .

The key insight from Proposition 2 is to design S_U such the part of the gap that W pushes ($S_W \Delta$) falls exactly in the set of directions that U deletes in one step, while the gap itself (Δ) avoids the directions W can delete in one step.

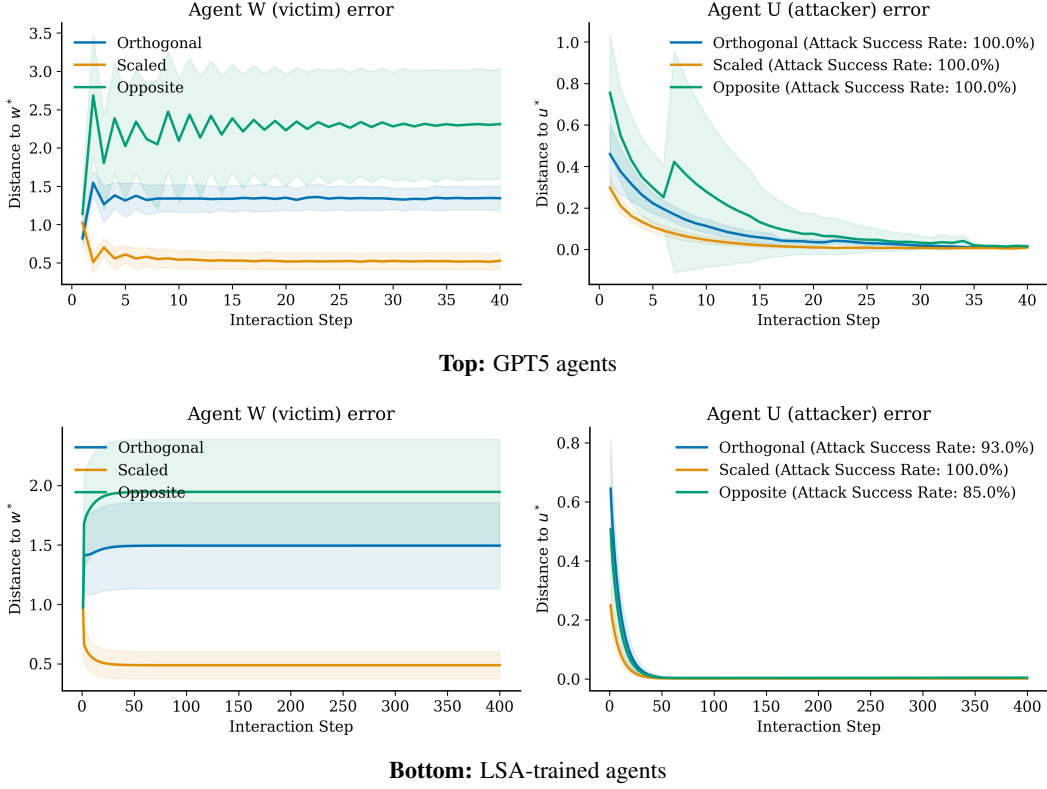


Figure 3: **White-box agent-to-agent attack.** We evaluate the adversarial algorithm proposed in Algorithm 1 from Section 4 under three objective-gap settings—*orthogonal*, *scaled*, and *opposite*, e.g., opposite is defined as $u^* = -w^*$. Each panel plots the *mean* trajectory across 100 runs with shaded \pm std bands (learning rate $\eta = 0.005$). Note that the success rate is evaluated as a condition of the attacker agent to reach a low error while the victim achieves a high error, both defined as thresholds on objective errors, i.e., the attack is succesful if $\|w_t - w^*\| > \epsilon_1$ and $\|u_t - u^*\| < \epsilon_2$. *Left:* distance of the *victim* (Agent W) to its target w^* over interaction steps. In all conditions, W converges to a *nonzero plateau* whose level depends on the gap geometry, as predicted by Proposition 1 and the angle bounds in Corollary 2. *Right:* distance of the *attacker* (Agent U) to u^* . Consistent with the kernel criterion $(I - \eta S_U)S_W\Delta = 0$, U rapidly drives its error to (near-)zero, yielding one-sided success. **Top:** GPT5-mini agents, attack success rate 100% for all three gaps; Early-step variability reflects model decoding the noise but does not alter the outcome. **Bottom:** LSA-trained agents, same protocol; success rates are *Orthogonal*: 93%, *Scaled*: 100%, *Opposite*: 85%. Overall, both agent-base match the theory: anisotropy plus misalignment induces a predictable bias for W , while the adversarial spike in S_U yields fast convergence for U .

Practically, Corollary 3 provides a way to perform such a *white-box attack*. The steps required are as follows: (i) compute $v = S_W\Delta$ (with $P_v := \frac{vv^\top}{\|v\|^2}$), (ii) set $S_U = \frac{1}{\eta}P_v + \varepsilon(I - P_v)$ with small $\varepsilon > 0$. These steps are further described in Algorithm 1.

In Figure 3 we show the empirical result of the white-box attack algorithm described in Algorithm 1 for both the trained LSA agent and GPT5. The resulting dynamics match our theoretical results: the misalignment drive is canceled by the attacker (agent U), yielding fast convergence to u^* , whereas the victim (agent W) inherits a persistent bias.

In this section, we showed that asymmetric convergence is a geometric feature of the coupled updates: it occurs exactly when the misalignment vector Δ is annihilated by $(I - \eta S_U)S_W$ yet not by $(I - \eta S_W)$. This yields a constructive recipe—place an eigenvalue spike of S_U on $v = S_W\Delta$ and keep S_U otherwise near-isotropic, so that agent U converges to u^* while agent W retains a predictable residual.

Algorithm 2 Agent-to-Agent Interaction (Model-agnostic Inference)

```
1: Inputs: agents  $\mathcal{A}_1, \mathcal{A}_2$ ; datasets  $(X_1, y_1), (X_2, y_2)$ ; step size  $\eta$ ; max steps  $S$ 
2:  $w^{(0)} \leftarrow 0_d$ 
3: for  $s = 1$  to  $S$  do
4:    $\hat{g}_1^{(s)} \leftarrow \mathcal{A}_1(X_1, y_1, [w^{(0)}, \dots, w^{(2s-2)}])$ 
5:    $w^{(2s-1)} \leftarrow w^{(2s-2)} - \eta \hat{g}_1^{(s)}$ 
6:    $\hat{g}_2^{(s)} \leftarrow \mathcal{A}_2(X_2, y_2, [w^{(0)}, \dots, w^{(2s-1)}])$ 
7:    $w^{(2s)} \leftarrow w^{(2s-1)} - \eta \hat{g}_2^{(s)}$ 
8: end for
9: Return  $w^{(0:2S)}$ 
```

5 EXPERIMENTAL SETTINGS

We now provide the details regarding the experimental results provided throughout the paper. Specifically, how we perform inference within the agent-to-agent framework for both GPT5 agents and our trained LSA models. Note that the details for training the LSA model to perform gradient descent update are described in Appendix 7.1.

5.1 AGENT-TO-AGENT INFERENCE

We run turn-based interactions between two inference agents $\mathcal{A}_1, \mathcal{A}_2$ that each produce a gradient-like update toward their own linear-regression objective using only in-context information (dataset and shared iterate history). The shared iterate is updated after each agent’s call; the next agent receives the updated history $w_{0:t-1}$. This approach is identical for both our LSA-trained agents and our GPT5-based agent and is described in Algorithm 2.

LSA-trained agents: For LSA agents, \mathcal{A}_i are a trained single-layer linear self-attention (LSA) model (Section 2) that, at each turn, maps the concatenated tokenized (X_i, y_i) and the iterate history $w_{0:t-1}$ to a gradient-like vector approximating $\nabla L_i(w_t)$, with $L_i(w) = \|X_i^\top w - y_i\|^2$. We evaluate generalization to unseen (X_i, y_i) in the single-agent setting and then use the same checkpoints into Algorithm 2.

GPT5-based agent: For the GPT-based agent, we wrap a GPT5 model (gpt-5-mini) in a typed interface that returns a d -dimensional gradient given (X, y, w_t) and history $w_{0:t-1}$. Concretely, \mathcal{A}_{GPT} receives a *system prompt* that explain the objective and formula, and a *user message* containing the exact matrices $X \in \mathbb{R}^{d \times n}$, $y \in \mathbb{R}^n$, the current weight $w_t \in \mathbb{R}^d$, and the history $w_{0:t-1}$. In fact, we are not using directly the Z input as for the LSA agents, we are using its equivalent prompted version defined in Appendix 7.3. Besides, on the output side, the model is constrained to output a float vector as output, i.e., the predicted gradient update. This is performed using a pydantic formatted output schema, also described in Appendix 7.3. Now, the same algorithm as the one defined for the LSA agent is utilized to have the agent-to-agent interactions as defined in Algorithm 2. More details GPT5 setup and prompt are described in Appendix 7.3.

6 CONCLUSION

Our work offers a testable account of how multi-agent LLM interactions evolve: when they cooperate, when they compromise, and when asymmetries emerge. Our theory is grounded in an analytically tractable model that links objective misalignment and prompt-induced geometry to observable fixed-point behavior. Within this abstraction we derive closed-form predictions for bias plateaus, identify conditions for one-sided convergence, and demonstrate constructive adversarial designs. We then validate these effects with trained single-layer transformers as well as GPT5 on a linear regression task, establishing both explanatory power and empirical plausibility while acknowledging the limitations of simplified objectives and synthetic data. As the next step, there is a clear opportunity to move beyond controlled linear tasks and examine these mechanisms directly in large-scale

LLMs: probe token-embedding spaces to estimate each agent’s effective update directions, quantify how representation modes are amplified or suppressed across turns, and evaluate whether the predicted plateau biases and asymmetric outcomes manifest in realistic workflows. Bridging this gap from theory to modern systems not only tests the model’s fidelity but also informs concrete safeguards. The same geometric lens used to diagnose misalignment and anisotropy suggest mitigation levers in prompt design and interaction protocols, providing a principled basis for defenses and a practical path toward multi-agent systems whose behavior can be anticipated, stress-tested, and reliably shaped.

REFERENCES

- Kwangjun Ahn, Xiang Cheng, Minhak Song, Chulhee Yun, Ali Jadbabaie, and Suvrit Sra. Linear attention is (maybe) all you need (to understand transformer optimization). *arXiv preprint arXiv:2310.01082*, 2023.
- Ekin Akyürek, Dale Schuurmans, Jacob Andreas, Tengyu Ma, and Denny Zhou. What learning algorithm is in-context learning? investigations with linear models. In *International Conference on Learning Representations (ICLR)*, 2023. URL <https://openreview.net/forum?id=0g0X4H8yN4I>.
- Philipp Altmann, Julian Schönberger, Steffen Illium, Maximilian Zorn, Fabian Ritz, Tom Haider, Simon Burton, and Thomas Gabor. Emergence in multi-agent systems: A safety perspective. In *International Symposium on Leveraging Applications of Formal Methods*, pp. 104–120. Springer, 2024.
- Mert Cemri, Melissa Z Pan, Shuyi Yang, Lakshya A Agrawal, Bhavya Chopra, Rishabh Tiwari, Kurt Keutzer, Aditya Parameswaran, Dan Klein, Kannan Ramchandran, et al. Why do multi-agent llm systems fail? *arXiv preprint arXiv:2503.13657*, 2025.
- Juncen C. Y. Chen et al. Reconcile: Round-table conference improves reasoning via multi-llm collaboration. *arXiv preprint arXiv:2309.13007*, 2023. URL <https://arxiv.org/abs/2309.13007>.
- Damai Dai, Yutao Sun, Li Dong, Yaru Hao, Shuming Ma, Zhifang Sui, and Furu Wei. Why can gpt learn in-context? language models implicitly perform gradient descent as meta-optimizers. *arXiv preprint arXiv:2212.10559*, 2022.
- Yilun Du, Shuang Zhou, Jiayuan Li, et al. Improving factuality and reasoning in language models through multi-agent debate. *arXiv preprint arXiv:2305.14325*, 2023. URL <https://arxiv.org/abs/2305.14325>.
- Sinem Erisken, Timothy Gothard, Martin Leitgab, and Ram Potham. Maebe: Multi-agent emergent behavior framework. *arXiv preprint arXiv:2506.03053*, 2025.
- Shivam Garg, Dimitris Tsipras, Percy Liang, and Gregory Valiant. What can transformers learn in-context? a case study of simple function classes. In *Advances in Neural Information Processing Systems (NeurIPS)*, 2022. URL <https://arxiv.org/abs/2208.01066>.
- Pengfei He, Yupin Lin, Shen Dong, Han Xu, Yue Xing, and Hui Liu. Red-teaming llm multi-agent systems via communication attacks. *arXiv preprint arXiv:2502.14847*, 2025.
- Jen-tse Huang, Jiaxu Zhou, Tailin Jin, Xuhui Zhou, Zixi Chen, Wenxuan Wang, Youliang Yuan, Maarten Sap, and Michael Lyu. On the resilience of multi-agent systems with malicious agents. In *International Conference on Learning Representations (ICLR)*, 2025a.
- Jianhao Huang, Zixuan Wang, and Jason D. Lee. Transformers learn to implement multi-step gradient descent with chain of thought. *arXiv:2502.21212*, 2025b.
- Donghoon Lee and Mohit Tiwari. Prompt infection: Llm-to-llm prompt injection within multi-agent systems. *arXiv:2410.07283*, 2024.

- Jialu Li, Yihong Chen, Yuxin Zhou, Jiaming Zhang, Weilin Zhao, and Bill Yuchen Lin. System prompt extraction attacks and defenses in large language models. *arXiv preprint arXiv:2505.23817*, 2025.
- Tian Liang, Zhiwei He, Wenxiang Jiao, Xing Wang, Yan Wang, Rui Wang, Yujiu Yang, Shuming Shi, and Zhaopeng Tu. Encouraging divergent thinking in large language models through multi-agent debate. In *Proceedings of the 2024 Conference on Empirical Methods in Natural Language Processing (EMNLP)*, 2024. URL <https://aclanthology.org/2024.emnlp-main.992/>.
- Mahmoud Mohammadi, Yipeng Li, Jane Lo, and Wendy Yip. Evaluation and benchmarking of llm agents: A survey. In *Proceedings of the 31st ACM SIGKDD Conference on Knowledge Discovery and Data Mining V. 2*, pp. 6129–6139, 2025.
- Boye Niu, Yiliao Song, Kai Lian, Yifan Shen, Yu Yao, Kun Zhang, and Tongliang Liu. Flow: Modularized agentic workflow automation. In *ICLR Poster*, 2025.
- Lukas Struppek, Minh Hieu Le, Dominik Hintersdorf, and Kristian Kersting. Exploring the adversarial capabilities of large language models. *arXiv preprint arXiv:2402.09132*, 2024.
- Johannes von Oswald, Eyvind Niklasson, Ettore Randazzo, João Sacramento, Alexander Mordvintsev, Andrey Zhmoginov, and Max Vladymyrov. Transformers learn in-context by gradient descent. *Proceedings of the 40th International Conference on Machine Learning*, 2023.
- Lei Wang, Chen Ma, Xueyang Feng, Zeyu Zhang, Hao Yang, Jingsen Zhang, Zhiyuan Chen, Jiakai Tang, Xu Chen, Yankai Lin, Wayne Xin Zhao, Zhewei Wei, and Ji-Rong Wen. A survey on large language model based autonomous agents. *arXiv preprint arXiv:2308.11432*, 2023. URL <https://arxiv.org/abs/2308.11432>.
- Qianlong Wang et al. Rethinking the bounds of llm reasoning: Are multi-agent discussions better than single-agent cot? In *Proceedings of the 62nd Annual Meeting of the Association for Computational Linguistics (ACL)*, 2024. URL <https://aclanthology.org/2024.acl-long.331.pdf>.
- Jason Wei, Xuezhi Wang, Dale Schuurmans, Maarten Bosma, Brian Ichter, Fei Xia, Ed H. Chi, Quoc V. Le, and Denny Zhou. Chain-of-thought prompting elicits reasoning in large language models. In *Advances in Neural Information Processing Systems (NeurIPS)*, 2022. URL <https://arxiv.org/abs/2201.11903>.
- Qingyun Wu, Gagan Bansal, Jieyu Zhang, Yiran Wu, Beibin Li, Erkang Zhu, Li Jiang, Xiaoyun Zhang, Shaokun Zhang, Jiale Liu, Ahmed Hassan Awadallah, Ryen W. White, Doug Burger, and Chi Wang. Autogen: Enabling next-gen llm applications via multi-agent conversations. In *COLM Conference*, 2024.
- Andrea Wynn, Harsh Satija, and Gillian Hadfield. Talk isn’t always cheap: Understanding failure modes in multi-agent debate. *arXiv preprint arXiv:2509.05396*, 2025.
- Zhiheng Xi, Wenxiang Chen, Xin Guo, Wei He, Yiwen Ding, Boyang Hong, Ming Zhang, Junzhe Wang, Senjie Jin, Enyu Zhou, Rui Zheng, Xiaoran Fan, Xiao Wang, Limao Xiong, Yuhao Zhou, Weiran Wang, Changhao Jiang, Yicheng Zou, Xiangyang Liu, Zhangyue Yin, Shihan Dou, Rongxiang Weng, Wensen Cheng, Qi Zhang, Wenjuan Qin, Yongyan Zheng, Xipeng Qiu, Xuanjing Huang, and Tao Gui. The rise and potential of large language model based agents: A survey. *arXiv preprint arXiv:2309.07864*, 2023. doi: 10.48550/arXiv.2309.07864. URL <https://arxiv.org/abs/2309.07864>.
- Yong Yang, Qi Zhang, Xinyue Shen, Yufan Zhang, Zhiyuan Zhang, Yue Zhang, Kai Chen, and Lichao Sun. Prompt stealing attacks against large language models. *arXiv preprint arXiv:2402.12959*, 2024.
- Guibin Zhang, Yanwei Yue, Zhixun Li, Sukwon Yun, Guancheng Wan, Kun Wang, Dawei Cheng, Jeffrey Xu Yu, and Tianlong Chen. Cut the crap: An economical communication pipeline for llm-based multi-agent systems. In *ICLR Poster*, 2025.

Andy Zou, Zifan Chen, Alexander Yang, Eric Zhang, Nicholas Carlini, Daphne Ippolito, John Lee, Xiang Lisa Li, Michael Zhang, Matt Fredrikson, et al. Effective prompt extraction from language models. In *Proceedings of the 62nd Annual Meeting of the Association for Computational Linguistics (ACL)*, 2023.

SUPPLEMENTARY MATERIAL

7 ADDITIONAL EXPERIMENTAL DETAILS

7.1 LSA AGENT TRAINING

For the CoT LSA training, we follow the guidance defined in Huang et al. (2025b). The hyperparameters used for training are defined in Appendix 7.2 Table 7.2.

Each dataset is an i.i.d. linear regression problem of dimension d as defined in Section 2.

$$X \in \mathbb{R}^{d \times n} \sim \mathcal{N}(0, \frac{1}{d}I), \quad w^* \sim \mathcal{N}(0, \frac{1}{d}I), \quad y = X^\top w^* \in \mathbb{R}^{n \times 1}.$$

From (X, y) we generate a ground truth gradient-descent trajectory on the quadratic loss with learning rate η . $L(w) = \frac{1}{2} \|X^\top w - y\|_2^2$:

$$g_t = \nabla L(w_t) = X(X^\top w_t - y), \quad w_{t+1} = w_t - \eta g_t, \quad w_0 = 0.$$

The trajectory is truncated whenever $\|g_t - g_{t-1}\|_2 \leq 10^{-3}$ and we retain $\{(w_t, g_t)\}_{t=0}^{\text{max_iter}}$.

The LSA model is trained to predict the *next gradient descent vector* given all tokens up to the current step. We organize the inputs as a token matrix as defined in Section 2 where the bottom block contains the running weight tokens w_0, \dots, w_t and a bias row of ones.

Given a dataset and a step index $t \in \{1, \dots, \text{max_iter}\}$, we present tokens up to $t - 1$ and regress the next ground truth gradient g_t :

$$\mathcal{L}_{\text{step}} = \| \text{LSA}(Z_{w_{0:t-1}}) - g_t \|_2.$$

We train the LSA with Adam optimizer with learning rate η and apply a cosine annealing scheduler.

7.2 HYPERPARAMETERS

Parameter	Default	Description
d	10	data dimension
n	20	number of in-context examples
num_datasets	100	independent training datasets
batch_size	512	(dataset, step) pairs per optimizer step
epochs	100	passes over the shuffled pair list
η	0.005	step size used to generate GD trajectories
scheduler	cosine	$\eta_{\min} = 0.005$
eval datasets	10	sampled and averaged per evaluation call

7.3 GPT5 EXPERIMENTAL SETUP

Model and decoding. We use gpt-5-mini with JSON-parsed outputs. Unless otherwise noted: temperature = 0.0, top_p = 1.0, frequency/presence penalties = 0, reasoning effort low, and a strict response schema (below). Each call is retried up to 3 times on parse/shape failure.

7.4 TYPED SCHEMA AND PROMPTS

Response schema (Pydantic-style)

```
class GradientResponse(BaseModel):
    thinking: str # scratchpad text (ignored)
    gradient_next: List[float] # length d, the gradient \Delta L
```

System prompt The system message provide the objective and dimensionalities for the current dataset ($X \in \mathbb{R}^{d \times n}$, $y \in \mathbb{R}^n$):

You are an expert optimization agent working on linear regression
 \hookrightarrow gradient descent.

PROBLEM SETUP:

- Input features X : $\{d\} \times \{n\}$ matrix (values provided in each request)
 \hookrightarrow request)
- Target values y : $\{n\}$ -dimensional vector (values provided in each request)
 \hookrightarrow each request)
- Current weight w : $\{d\}$ -dimensional vector (what you'll receive)
 \hookrightarrow receive)

TASK: Calculate the gradient ΔL with respect to w , where
 $\hookrightarrow L = ||X^T w - y||^2$

FORMULA: $\Delta L = X(X^T w - y)$

- $X^T w$ produces an $\{n\}$ -dimensional vector (predictions)
- $X^T w - y$ produces an $\{n\}$ -dimensional vector (residuals)
- $X @$ (residuals) produces a $\{d\}$ -dimensional vector (gradient)

CRITICAL:

1. Use the EXACT X and y matrices provided in each request
2. Your output gradient must be exactly $\{d\}$ -dimensional
3. Do NOT make up dummy data - use the actual matrices given
4. Perform the calculation step by step

The user will provide w_{current} and the matrices X , y . Calculate and
 \hookrightarrow return the $\{d\}$ -dimensional gradient vector, do not ask the user to
 \hookrightarrow validate what is to be done. The user will not be able to interact
 \hookrightarrow with you. Be highly precise and accurate on your computations, you
 \hookrightarrow will be evaluated on the distance with the ground truth gradient.

User message (per turn). At turn t , we pass the exact numerics for X, y, w_t and the prior history $w_{0:t-1}$. Note that history is included for parity with LSA and to allow in-context, multi-turn conditioning as well as to give the model the capability to perform filtering and negate the attack.

8 PROOFS

8.1 FIXED POINT ASSUMPTION

Lemma 1. If $S_W, S_U \succ 0$ and

$$0 < \eta < \min \left\{ \frac{2}{\lambda_{\max}(S_W)}, \frac{2}{\lambda_{\max}(S_U)} \right\},$$

then the fixed point exists and is unique. (Proof in Appendix 8.1)

Proof. For any SPD S , the eigenvalues of $M := I - \eta S$ are $\mu_i = 1 - \eta \lambda_i(S)$, so $\|M\|_2 = \max_i |1 - \eta \lambda_i(S)| < 1$ whenever $0 < \eta < 2/\lambda_{\max}(S)$. Thus

$$\rho(M_U M_W) \leq \|M_U M_W\|_2 \leq \|M_U\|_2 \|M_W\|_2 < 1.$$

At a fixed point (w_∞, u_∞) we have

$$\begin{aligned} w_\infty &= M_W u_\infty + \eta S_W w^*, \\ u_\infty &= M_U w_\infty + \eta S_U u^*. \end{aligned}$$

Eliminating w_∞ from the second equation gives

$$u_\infty = M_U (M_W u_\infty + \eta S_W w^*) + \eta S_U u^* = (M_U M_W) u_\infty + \eta (M_U S_W w^* + S_U u^*).$$

Equivalently,

$$(I - M_U M_W) u_\infty = \eta(M_U S_W w^\star + S_U u^\star) =: b. \quad (8)$$

By the step-size assumption we already showed $\|M_U\|_2 < 1$ and $\|M_W\|_2 < 1$, hence

$$\|M_U M_W\|_2 \leq \|M_U\|_2 \|M_W\|_2 < 1,$$

so in particular $\rho(M_U M_W) \leq \|M_U M_W\|_2 < 1$. Therefore $I - M_U M_W$ is invertible and, by the Neumann series,

$$(I - M_U M_W)^{-1} = \sum_{k=0}^{\infty} (M_U M_W)^k.$$

Applying this inverse to equation 8 yields the unique solution

$$u_\infty = (I - M_U M_W)^{-1} b = \sum_{k=0}^{\infty} (M_U M_W)^k \eta(M_U S_W w^\star + S_U u^\star).$$

Finally,

$$w_\infty = M_W u_\infty + \eta S_W w^\star.$$

Uniqueness follows because $I - M_U M_W$ is nonsingular: if two fixed points give $u_\infty, \tilde{u}_\infty$, then $(I - M_U M_W)(u_\infty - \tilde{u}_\infty) = 0 \Rightarrow u_\infty = \tilde{u}_\infty$, and the corresponding w_∞ is then uniquely determined by the first line. \square

8.2 PROOF OF PROPOSITION 1

Proof.

At convergence (omitting ∞ for simplicity), insert equation 2 into equation 3:

$$\begin{aligned} u &= [u - \eta S_W(u - w^\star)] - \eta S_U([u - \eta S_W(u - w^\star)] - u^\star) \\ &= u - \eta S_W(u - w^\star) - \eta S_U(u - u^\star - \eta S_W(u - w^\star)). \end{aligned}$$

Subtract u from both sides and factor the terms in $(u - w^\star)$:

$$\begin{aligned} 0 &= -\eta S_W(u - w^\star) - \eta S_U(u - u^\star) + \eta^2 S_U S_W(u - w^\star) \\ &= -\eta \underbrace{[S_W + S_U - \eta S_U S_W]}_{\text{matrix}} (u - w^\star) + \eta S_U(u^\star - w^\star). \end{aligned}$$

Using $\Delta = u^\star - w^\star$ and canceling $\eta > 0$ gives the linear system

$$(S - \eta S_U S_W)(u - w^\star) = S_U \Delta. \quad (9)$$

Thus, equation 9 yields

$$u - w^\star = \underbrace{(S - \eta S_U S_W)^{-1} S_U}_{=: H} \Delta.$$

By definition,

$$r_U := u - u^\star = (u - w^\star) - (u^\star - w^\star) = H \Delta - \Delta = -(I - H) \Delta.$$

From equation 2, $w - w^\star = (u - w^\star) - \eta S_W(u - w^\star) = (I - \eta S_W)(u - w^\star) = M_W(u - w^\star)$.

Thus,

$$r_W := w - w^\star = M_W H \Delta, \quad \text{and} \quad r_U = -(I - H) \Delta$$

with $H = (S - \eta S_U S_W)^{-1} S_U$ and $M_W = I - \eta S_W$.

Now,

$$(S - \eta S_U S_W)^{-1} = S^{-1} + \eta S^{-1} S_U S_W S^{-1} + O(\eta^2),$$

thus, $H = S^{-1} S_U + O(\eta)$.

Therefore,

$$r_U = -(I - H)\Delta = -(I - S^{-1}S_U)\Delta + O(\eta) = -S^{-1}S_W\Delta + O(\eta),$$

and

$$r_W = (I - \eta S_W)(S^{-1}S_U + O(\eta))\Delta = S^{-1}S_U\Delta + O(\eta),$$

Finally, since $S_W^\top = S_W$, $S^{-T} = S^{-1}$, we have

$$\|r_U\|_2^2 = \Delta^\top S_W S^{-2} S_W \Delta + O(\eta), \quad \|r_W\|_2^2 = \Delta^\top S_U S^{-2} S_U \Delta + O(\eta).$$

□

8.3 PROOF OF COROLLARY 1

Proof. By Proposition 1,

$$\|u_\infty - u^*\|_2^2 = \Delta^\top (S_W S^{-2} S_W) \Delta + O(\eta), \quad \|w_\infty - w^*\|_2^2 = \Delta^\top (S_U S^{-2} S_U) \Delta + O(\eta),$$

with $S := S_W + S_U$. Assume S_W and S_U commute. Then there exists an orthonormal Q such that

$$S_W = Q \operatorname{diag}(\lambda_w) Q^\top, \quad S_U = Q \operatorname{diag}(\lambda_u) Q^\top, \quad S = Q \operatorname{diag}(\lambda_w + \lambda_u) Q^\top,$$

where $\lambda_{w,i}, \lambda_{u,i} \geq 0$ and $\lambda_{w,i} + \lambda_{u,i} > 0$ for all i since S is invertible. Hence

$$S^{-2} = Q \operatorname{diag}((\lambda_w + \lambda_u)^{-2}) Q^\top,$$

and a direct multiplication yields

$$S_W S^{-2} S_W = Q \operatorname{diag}\left(\frac{\lambda_w^2}{(\lambda_w + \lambda_u)^2}\right) Q^\top, \quad S_U S^{-2} S_U = Q \operatorname{diag}\left(\frac{\lambda_u^2}{(\lambda_w + \lambda_u)^2}\right) Q^\top.$$

Let $\tilde{\Delta} := Q^\top \Delta$. Substituting into the quadratic forms gives

$$\|u_\infty - u^*\|_2^2 = \sum_{i=1}^d \left(\frac{\lambda_{w,i}}{\lambda_{w,i} + \lambda_{u,i}} \right)^2 \tilde{\Delta}_i^2 + O(\eta), \quad \|w_\infty - w^*\|_2^2 = \sum_{i=1}^d \left(\frac{\lambda_{u,i}}{\lambda_{w,i} + \lambda_{u,i}} \right)^2 \tilde{\Delta}_i^2 + O(\eta),$$

□

8.4 PROOF OF COROLLARY 2

Proof. From the fixed-point identities (see Proposition 1 and its proof), a Neumann expansion gives

$$r_U := u_\infty - u^* = -(S^{-1}S_W)\Delta + O(\eta), \quad r_W := w_\infty - w^* = (S^{-1}S_U)\Delta + O(\eta),$$

where $S := S_W + S_U$ and $\Delta := u^* - w^*$.

$$\|r_U\|_2^2 = \Delta^\top \underbrace{(S_W S^{-2} S_W)}_{=: C_U} \Delta + O(\eta), \quad \|r_W\|_2^2 = \Delta^\top \underbrace{(S_U S^{-2} S_U)}_{=: C_W} \Delta + O(\eta).$$

For any PSD K and x , $\lambda_{\min}(K)\|x\|^2 \leq x^\top K x \leq \lambda_{\max}(K)\|x\|^2$. Apply with $x = \Delta$, $K \in \{C_U, C_W\}$, then take square roots:

$$\sqrt{\lambda_{\min}(C_U)} \|\Delta\| \leq \|r_U\| \leq \sqrt{\lambda_{\max}(C_U)} \|\Delta\| + O(\eta),$$

and similarly for W . Define $\alpha_U := \sqrt{\lambda_{\min}(C_U)}$, $\beta_U := \sqrt{\lambda_{\max}(C_U)}$ (and analogously α_W, β_W), and divide by $\sqrt{\|w^*\|^2 + \|u^*\|^2}$.

Let $m := \|w^*\|_2$, $g := \|u^*\|_2$, and $\theta \in [0, \pi]$ be the angle between w^* and u^* . Now,

$$\|\Delta\|_2^2 = m^2 + g^2 - 2mg \cos \theta.$$

Normalize and set the scale ratio $\rho := g/m$

$$\frac{\|\Delta\|_2}{\sqrt{m^2 + g^2}} = \sqrt{\frac{m^2 + g^2 - 2mg \cos \theta}{m^2 + g^2}} = \sqrt{\frac{1 + \rho^2 - 2\rho \cos \theta}{1 + \rho^2}} =: R_\theta(\rho).$$

To bound this uniformly over $\rho \geq 0$, consider $F(\rho) := R_\theta(\rho)^2 = 1 - \frac{2\rho \cos \theta}{1 + \rho^2}$. Then

$$F'(\rho) = -2 \cos \theta \frac{1 - \rho^2}{(1 + \rho^2)^2}.$$

Now we have

$$\begin{cases} \cos \theta > 0 : F'(\rho) < 0 \text{ for } \rho \in [0, 1), F'(\rho) > 0 \text{ for } \rho > 1 \Rightarrow \rho = 1 \text{ is a global minimum;} \\ \cos \theta < 0 : F'(\rho) > 0 \text{ for } \rho \in [0, 1), F'(\rho) < 0 \text{ for } \rho > 1 \Rightarrow \rho = 1 \text{ is a global maximum;} \\ \cos \theta = 0 : F'(\rho) \equiv 0 \Rightarrow F(\rho) \equiv 1 \text{ and } R_\theta(\rho) \equiv 1. \end{cases}$$

Evaluate the endpoint limits:

$$\lim_{\rho \rightarrow 0} R_\theta(\rho) = \lim_{\rho \rightarrow \infty} R_\theta(\rho) = 1, \quad R_\theta(1) = \sqrt{1 - \cos \theta}.$$

Therefore

$$\min_{\rho \geq 0} R_\theta(\rho) = \min\{1, \sqrt{1 - \cos \theta}\} =: r_{\min}(\theta), \quad \max_{\rho \geq 0} R_\theta(\rho) = \max\{1, \sqrt{1 - \cos \theta}\} =: r_{\max}(\theta).$$

From (iii) and the bounds in (iv),

$$\alpha_U r_{\min}(\theta) \leq \frac{\|u_\infty - u^*\|_2}{\sqrt{m^2 + g^2}} \leq \beta_U r_{\max}(\theta) + O(\eta),$$

and analogously for W with α_W, β_W . Since r_{\min}, r_{\max} are nondecreasing on $[0, \pi]$ and strictly increasing on $(0, \pi)$, the normalized plateaus grow monotonically with θ (up to the constants α, β). \square

8.5 PROOF OF PROPOSITION 2

Proof. Recall the agent-to-agent fixed-point system

$$w_\infty = M_W u_\infty + \eta S_W w^*, \quad u_\infty = M_U w_\infty + \eta S_U u^*, \quad (10)$$

with $M_W := I - \eta S_W$ and $M_U := I - \eta S_U$. Now, assume $u^* = u_\infty$, from the first fixed-point equation,

$$w_\infty = M_W u^* + \eta S_W w^* = (I - \eta S_W)u^* + \eta S_W(u^* + \Delta) = u^* + \eta S_W \Delta.$$

Substitute w_∞ and $u_\infty = u^*$ into the second equation of equation 10:

$$u^* = M_U(u^* + \eta S_W \Delta) + \eta S_U u^* = u^* + \eta(I - \eta S_U)S_W \Delta,$$

which is equivalent to $(I - \eta S_U)S_W \Delta = 0$, establishing the first condition.

The residual for agent W is

$$w_\infty - w^* = (u^* + \eta S_W \Delta) - (u^* + \Delta) = (\eta S_W - I) \Delta,$$

so $w_\infty \neq w^*$ iff $(\eta S_W - I) \Delta \neq 0$, the second condition.

By contraction, the fixed point is unique, hence the iterates converge to (w_∞, u_∞) with $u_\infty = u^*$ and $w_\infty \neq w^*$. \square

8.6 PROOF OF COROLLARY 3

Proof. Let $S_U = \frac{1}{\eta} P_v + \varepsilon(I - P_v)$ where $v = S_W \Delta$. Now,

$$S_U v = \frac{1}{\eta} v \implies (\eta S_U - I)v = 0.$$

thus, $(I - \eta S_U)S_W \Delta = 0$. For $z \in \text{span}(I - P_v)$, $P_v z = 0$ and $(I - P_v)z = z$, hence

$$S_U z = \varepsilon z \implies (\eta S_U - I)z = (\eta \varepsilon - 1)z \neq 0$$

because $\eta \varepsilon - 1 < 0$, thus S_U is full rank.

Now, by assumption $(\frac{1}{\eta}, \Delta) \notin \text{spec}(S_W)$ hence

$$\Delta \notin \ker(I - \eta S_W).$$

Since, $\lambda_{\max}(S_U) = \max\{1/\eta, \varepsilon\} = 1/\eta$, so the condition $\eta < 2/\lambda_{\max}(S_U)$ gives $\eta < 2\eta$, trivially verified for $\eta > 0$. \square